AGU PUBLICATIONS

Geophysical Research Letters

RESEARCH LETTER
10.1002/2015GL065192

Key Points:
- Electron enhancements at geosynchronous orbit likely occur independently from magnetic storms
- Small Nsw and strong AE for prolonged time is essential
- Examining solar wind conditions in early recovery phase of storm is important

Correspondence to:
H.-J. Kim,
heekim@atmos.ucla.edu

Citation:
Kim, H.-J., L. Lyons, V. Pinto, C.-P. Wang, and K.-C. Kim (2015), Revisit of relationship between geosynchronous relativistic electron enhancements and magnetic storms, *Geophys. Res. Lett.*, *42*, doi:10.1002/2015GL065192.

Received 8 JUL 2015
Accepted 19 JUL 2015
Accepted article online 22 JUL 2015

Revisit of relationship between geosynchronous relativistic electron enhancements and magnetic storms

Hee-Jeong Kim[1], Larry Lyons[1], Victor Pinto[1], Chih-Ping Wang[1], and Kyung-Chan Kim[2]

[1]Department of Atmospheric and Oceanic Sciences, University of California, Los Angeles, California, USA, [2]Korea Astronomy and Space Science Institute, Daejeon, South Korea

Abstract We find evidence that magnetic storms are not only unnecessary for geosynchronous relativistic electron enhancements but also not directly relevant to the electron enhancements even if the enhancements are accompanied by magnetic storms. What is crucial for electron enhancements at geosynchronous orbit are sustained south-oriented or north-south fluctuating interplanetary magnetic field (IMF) B_z that drives sufficiently large substorm activity and small solar wind density N_{sw} that likely leads to low loss rate of relativistic electrons to the ionosphere and/or to the magnetopause for an extended time period. Specifically, almost all the abrupt, large electron increases in our data set took place under the condition of average $AE > 235$ nT and average $N_{sw} \leq 5\ cm^{-3}$. Examination of detailed time profiles clearly shows that electron flux starts to increase quite immediately with arrival of the right IMF and solar wind conditions, regardless of a magnetic storm, leaving the accompanied magnetic storms merely coincident.

1. Introduction

Large flux increases of MeV electrons at geosynchronous orbit are frequently referred to as a storm recovery phase phenomena, although it has long been known that relativistic electron enhancements sometimes do, and sometimes do not, occur in association with geomagnetic storms. However, relativistic electron increases are also closely related to high-speed solar wind streams. This, together with significant electron enhancements being seen during high V_{sw} periods that are not preceded by storms [*Lyons et al.*, 2005] and the frequent occurrence of storms that are not accompanied by electron enhancements [e.g., *Reeves*, 1998], suggests that storms may not be fundamental to production of geosynchronous relativistic electrons.

Here we revisit the topic of magnetic storms versus MeV electrons at geosynchronous orbit focusing on their relationship, not only determining why only some storms have flux enhancements but also investigating the possibility that electron flux enhancements at geosynchronous orbit are produced by distinct solar wind drivers which may be different from those that directly produce the main phase of magnetic storms. We first statistically identify characteristic solar wind and magnetosphere conditions observed during storms that accompany electron enhancements and then use example events to discuss that only those conditions, which can be present regardless of storms, play a crucial role in electron enhancements at geosynchronous orbit, while magnetic storms are merely often coincident.

2. Which Magnetic Storms can Have Geosynchronous MeV Electron Enhancements?

Figure 1 illustrates two remarkably similar, strong storms that have distinctively different recovery phase electron levels. Both are associated with fast ($V_{sw} > \sim 500$ km/s) solar wind streams with similar V_{sw} time profiles, though V_{sw} for Storm 2 is smaller. While fast streams are closely related with relativistic electron enhancements, events like Storm 2 are not rare. Our analysis will also provide an answer to why not every fast solar wind stream has electron enhancements.

Several parameters have been suggested to best separate storms that do and do not produce relativistic electrons. They include V_{sw} [e.g., *O'Brien et al.*, 2001], Pi1 [*Degtyarev et al.*, 2009], and Pc5 [*O'Brien et al.*, 2001; *Reeves et al.*, 2003] ULF wave power, and the *Ap* index [*Bühler and Desorgher*, 2002]. To identify crucial conditions, we perform statistical analysis similar to the earlier works. However, unlike most of these,

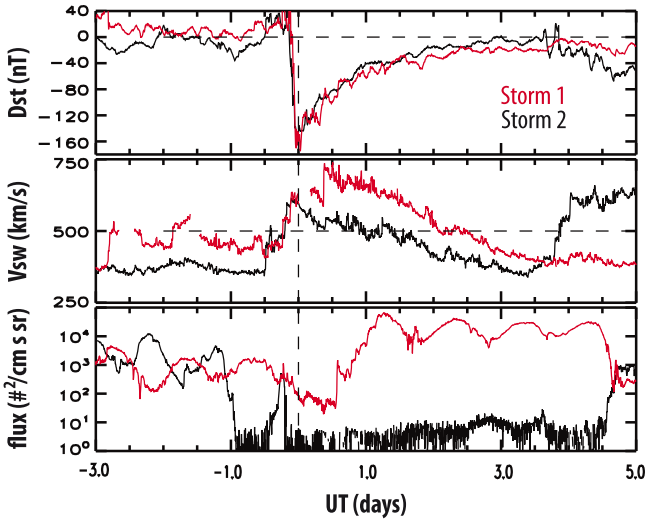

Figure 1. Storm 1 on 24 August 2005 and Storm 2 on 22 September 1999. (top) *Dst*, (middle) V_{sw}, and (bottom) >2 MeV electron fluxes from GOES 10. The dashed line indicates the time of Dst_{min}.

we focus on the solar wind and magnetosphere conditions for the early recovery phase when abrupt, large flux increases usually take place, as seen in Figure 1. Focusing only on the early recovery day is important for identifying the true relationship between storms and relativistic electrons, as discussed later.

We collected storms of $Dst_{min} < -50$ nT from 1996 to 2006. We obtained average >2 MeV electron fluxes for recovery day 1 (0.5 to 1.5 day after Dst_{min}) and for the prestorm day (−1.5 to −0.5 day) from GOES. For a given storm, if the recovery day 1 flux is >1000 (<100) $cm^{-2}\,s^{-1}\,sr^{-1}$ and 2 times larger (smaller) than the prestorm day flux, it is called a high (low) flux storm. We also regard as low-flux storms cases where the recovery day 1 flux is slightly larger than 100 $cm^{-2}\,s^{-1}\,sr^{-1}$ but is more than an order of magnitude lower than the prestorm flux. Similarly, we also include as high-flux storms cases where a rapid, large flux increase took place on the first recovery day but the daily average flux did not reach the cutoff value until the second day. A total of 65 high-flux and 62 low-flux storms were identified for the 11 year period. The Dst_{min} of these storms (not shown) indicates that enhancements can occur for any storm size, and for a given Dst_{min}, the expectations to have either low flux or high flux are roughly equal. Furthermore, the amount of flux increase or decrease did not show any clear storm size dependence. These are all consistent with previous reports [e.g., *Reeves et al.*, 2003].

To determine differences between the two storm types, we examined average solar wind and magnetosphere conditions during early recovery phase. Solar wind and interplanetary magnetic field (IMF) parameters (in GSM coordinates) are as mapped to the magnetopause in the OMNI database. Total time of south IMF B_z and averages of various quantities were computed for recovery day 1 for low-flux storms, and for the first day of flux enhancement for high-flux storms. The high-flux storm criteria assure that rapid, large flux increases started within ~1 day after $Dst_{min,}$ and averages were taken over the day from the start of large flux increase. Figure 2 shows probability density of total time of south B_z (in days), and averages of V_{sw}, N_{sw}, and *AE* for low-flux storms (blue) and high-flux storms (red). It is clear that the two types of storms are accompanied by quite different solar wind features. Figure 2a illustrates that low-flux storms have predominantly northward IMF during the first day of recovery. For all the low-flux storms, IMF B_z had a large northward turning mostly right after Dst_{min} and then stayed northward for an extended time period (> ~1 day). On the other hand, many of the high-flux storms had north-south fluctuating IMF, and thus almost all the high-flux storms had total south B_z time > ~0.4 day. Figure 2b shows that high-flux storms are associated with higher V_{sw}, which is already well known. Interestingly, the two probability density curves resemble each other, the curve for high-flux storms being shifted to higher V_{sw} by a factor of ~1.5. Based on the overlapped region of the two curves, high V_{sw} does not necessarily lead to flux enhancements. The low-flux storms having average $V_{sw} > 500$ km/s appeared to be associated with predominantly northward IMF during recovery day 1, which indicates that although V_{sw} contributes to electron flux dynamics, sufficient amount of southward IMF is also necessary.

Note that for all the high-flux storms, electron fluxes started to increase only after N_{sw} dropped below ~5 cm^{-3}, and it stayed small throughout the rapid, large flux increase. The continuously small N_{sw} gives average, recovery phase $N_{sw} < 5$ cm^{-3} for almost all the high-flux storms, whereas it can be any number for low-flux storms, as illustrated in Figure 2c, indicating that small N_{sw} is also a necessary (but not sufficient) condition for flux enhancements. The importance of low N_{sw} is likely attributable to its role in loss. *Borovsky and Denton* [2009] found that for high-speed stream-driven storms, there is considerable

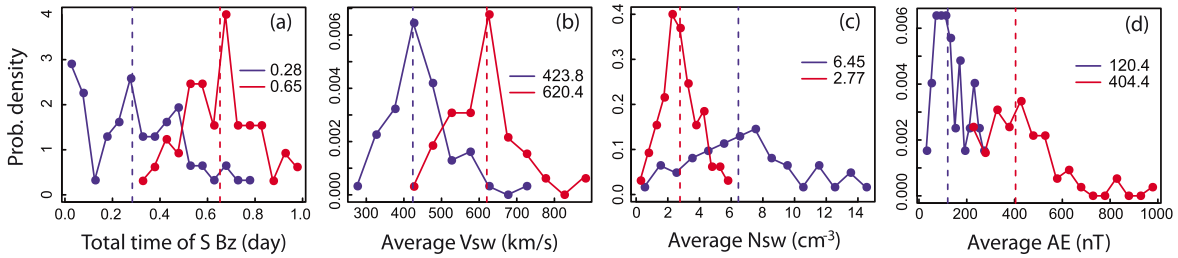

Figure 2. Probability density for (a) total time of south IMF B_z, (b) average V_{sw}, (c) average N_{sw}, and (d) average *AE* for high-flux storms in red and low-flux storms in blue. The dotted lines and the numbers in the legend in each panel indicate the median values.

spatial overlap of the superdense ion plasma sheet with plasmaspheric drainage plumes. This would lead to growth of electromagnetic ion-cyclotron waves that can cause relativistic electron precipitation loss. Since the superdense plasma sheet is associated with high N_{sw} [*Borovsky and Denton*, 2009], large N_{sw} would enhance such loss. On the other hand, large N_{sw} can also lead to relativistic electron loss to the magnetopause. Inward displacement of the magnetopause into the region of outer belt drift trajectories leads to electron loss [e.g., *Kim et al.*, 2008], which extends farther earthward than the drift shells that directly impact the magnetopause due to outward radial diffusion [*Shprits et al.*, 2006]. Apart from which loss process may be stronger, N_{sw} clearly plays a crucial role in electron loss. In particular, flux starting to increase only after N_{sw} drops below ~5 cm^{-3} indicates the condition of relativistic electron source starting to surpass loss.

Figure 2d shows probability density of average *AE*, which measures auroral electrojet activity and generally represents the strength of substorm activity. For low-flux storms, due to smaller V_{sw} and predominantly northward IMF, solar wind energy input is low, and thus, average *AE* is significantly smaller. This results in all the low-flux storms being associated with small average *AE*, the median average *AE* being more than 3 times smaller than that for high-flux storms. We also examined *Kp* and ground ULF index. *Kp* represents the disturbance intensity at subauroral and midlatitude regions. ULF index, defined as the logarithm of ULF wave power averaged over 1 h, reflects the intensity of magnetospheric Pc5 ULF wave activity [*Kozyreva et al.*, 2007]. While both ULF index and *Kp* are highly correlated with *AE*, *AE* is found to best discriminate between the high-flux storms and low-flux storms. This can be seen from Figure 3a, which gives prediction errors for each index. Here prediction error is defined as the ratio of number of events with false prediction to total number of events, representing how well a given threshold of an average index separates high- and low-flux storms. Figure 3a shows this error ratio versus changing index threshold. The minimum prediction error can be seen for average $AE = 235$ nT, for which 4 of the 65 high-flux storms have average $AE < 235$ nT and 5 of 62 low-flux storms have average $AE > 235$ nT. This gives an error ratio of (4+5)/(66+62) = ~7.6%. If we add the condition of average $N_{sw} = 5\ cm^{-3}$ as an additional threshold separating high- and low-flux storms, the error ratio becomes even smaller, ~2.4%.

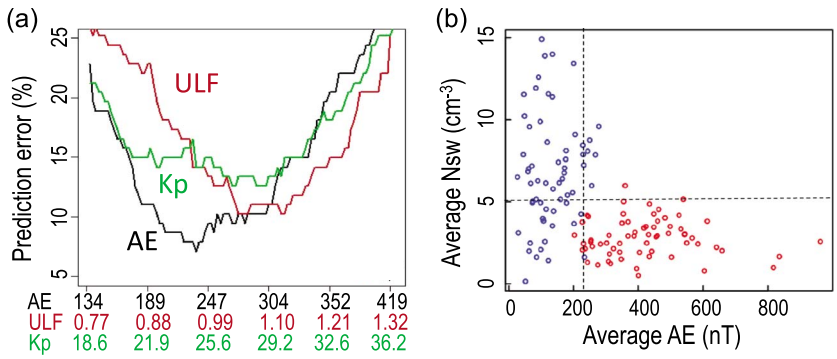

Figure 3. (a) Prediction error for average *AE*, average *Kp*, and average ULF index. Here we used *Kp* index in decimal scale (multiplied by 10) from the OMNI data set. (b) Distribution of high-flux storms (red) and low-flux storms (blue) in the parameter space of average *AE* and average N_{sw}. The two dotted lines indicate $AE = 235$ nT and $N_{sw} = 5\ cm^{-3}$.

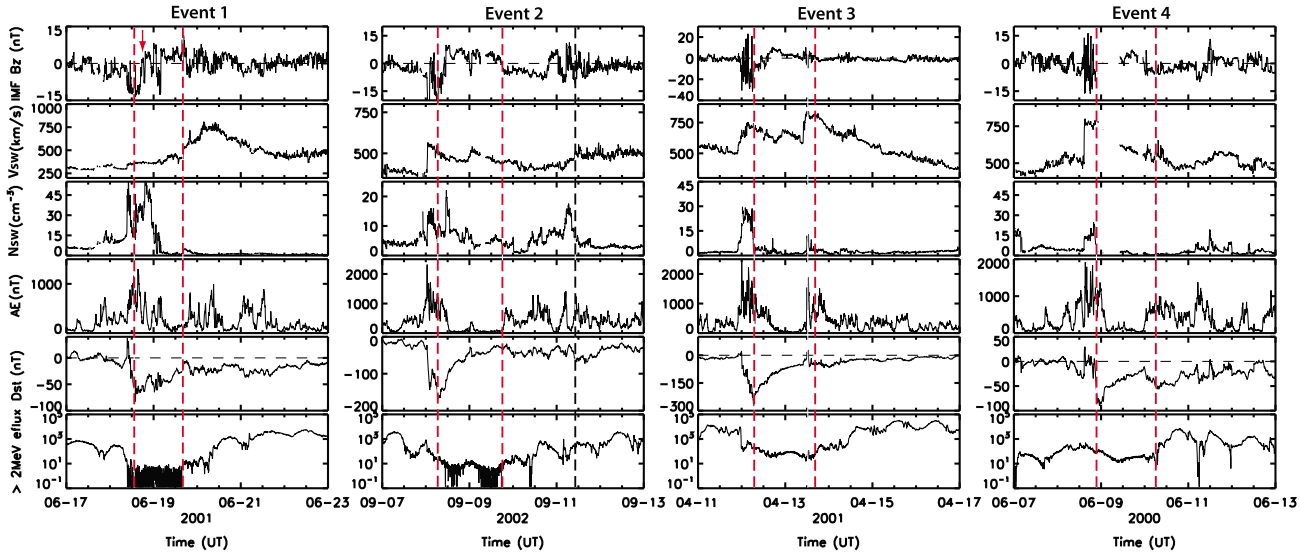

Figure 4. Four magnetic storms that were followed by large electron enhancements. Two red vertical lines in each panel indicate the times of storm peak and of start of electron flux increase, respectively. The black dashed line in Event 2 indicates the arrival of the new fast stream with predominantly southward, fluctuating IMF.

The result that *AE* is a better discriminator than ULF power is opposite to *O'Brien et al.* [2001]. They found that ULF power is more relevant than *AE* to electron enhancements by examining cross-correlation coefficients between the two parameters and the maximum fluxes for all magnetic storms. However, they adopted different averaging intervals, i.e., 12–36 h after Dst_{min} for ULF power and 0–48 h for *AE*. Had they used the same interval of 12–36 h (similar to our analysis) for both parameters, they would have obtained a result consistent with ours. Nonetheless, the low prediction error for ULF index in Figure 3a indicates that Pc5 ULF wave activity is closely related to electron enhancements, a result consistent with many previous studies [e.g., *Rostoker et al.*, 1998; *Elkington et al.*, 1999; *O'Brien et al.*, 2003].

The importance of sustained low N_{sw} and enhanced substorm activity for electron enhancements is illustrated in Figure 3b, where all events are plotted in the parameter space of average N_{sw} and average *AE*. The separation of the two types of storms is dramatic in this space. Almost all (~94%) high-flux storms are associated with average $AE > 235$ nT and average $N_{sw} \leq 5\ cm^{-3}$. The errors are from the uncertainty of the electron enhancement start time and the development of a second storm during the last part of the recovery day 1 for a few low-flux storms.

That only a small number of events are found in the upper right quadrant is attributable to the tendency for V_{sw} and N_{sw} to anticorrelate; that is, fast streams are low-density solar wind. Since high-speed streams having southward IMF always lead to high *AE*, the combination of low N_{sw} and high *AE* is much more likely to occur than the combination of high N_{sw} and high *AE*.

3. How Relatable Are Magnetic Storms and Geosynchronous MeV Electron Enhancements?

Unlike our present study, earlier statistical works often used a maximum value of electron flux within several days after Dst_{min} for determination of whether a storm has relativistic electrons or not. They also related conditions over a much longer time period spanning days prior to the storm main phase to the day of maximum electron flux in order to identify key drivers of relativistic electrons. As shown in the examples below, correlating magnetic storms (or/and solar wind/IMF conditions) and electron fluxes allowing such a long time lag may lead to misleading conclusions.

Figure 4 presents four storms, all followed by electron flux enhancements. The two dashed vertical lines in each panel indicate the times of storm peak and of start of flux increase. The times between the two lines are less than 2 days for all cases. If we adopt similar criteria to that normally used in earlier statistical studies, these storms would be regarded as accompanying relativistic electron flux increases. However, if

we examine the time profiles of solar wind/IMF parameters in detail, we see that these storms are not directly related to their following flux enhancements. For Event 1, as indicated by the arrow, B_z sharply turned northward just after Dst_{min}. Then after a couple of sharp, short southward excursions, B_z turned northward, accompanied by a sharp N_{sw} drop, and then stayed mostly northward for approximately a half day. During that time, *AE* was low and there is no sign of an electron flux increase. Only after B_z turned southward and underwent north-south fluctuations did the electron flux increase. This occurred just after the large V_{sw} jump at the second vertical line. This velocity jump brought an IMF having substantially different characteristics (much more rapid north-south changes) than the prior IMF. *AE* became large, and the electron flux started to increase almost simultaneously with the new IMF, indicating that this electron enhancement is not directly related to the solar wind condition that drove the preceding magnetic storm.

In Event 2, the IMF B_z sharply and largely turned northward after the storm peak and stayed north for ~1.5 days. Flux started to increase when B_z turned southward. This south B_z caused a ~20 nT drop in *Dst*, but previous statistical studies would identify this flux increase as a feature of the recovery phase of the preceding larger storm, rather than a response to the new southward IMF. Note that V_{sw} was below ~450 km/s during the prolonged south B_z interval, serving as one example of nonhigh-speed stream associated electron enhancements. The black dashed line indicates the abrupt arrival of a new solar wind stream with highly fluctuating, though mostly southward, IMF. Associated with this new solar wind feature, *AE* continued to be high and the electron flux continued to grow.

Event 3 shows a superstorm driven by a shock-magnetic cloud event. As the IMF rotated from south to north and stayed north for approximately a day, electron flux did not increase from its main phase drop. It started to increase only when a new fast stream with southward IMF arrived. Similar to Event 2, the flux increase could be incorrectly associated with the preceding superstorm. In Event 4, there was no large electron drop associated with the magnetic storm marked by the first dashed line, but large flux increase occurred about 1.5 days later. This flux enhancement could be claimed to have occurred during the recovery phase of the preceding storm, but the time profiles of IMF/solar wind show that they are not related. Electron flux started to increase when a subsequent high-speed stream brought southward IMF. Note that there was no large N_{sw} peak accompanying this stream, indicating that a large N_{sw} drop is not required for flux enhancements, but small N_{sw} itself is a necessary condition.

The examples in Figure 4, while not being the majority, are not rare. They can happen when multiple streams with different IMF characteristics arrive closely in time. For 6 of our 65 high-flux storms (~9%), electron enhancement appeared to be associated with a different solar wind stream from that which drove its preceding larger magnetic storm, and for about 11% of the events, determination of whether there was a new stream or not was ambiguous. Together with the observations that electron response is quite immediate to changes in IMF/solar wind, this occasional occurrence of close arrivals of multiple streams emphasizes the importance of examining detailed time profile for correct determination of the relationship between storms and electron enhancements.

Figure 4 suggests that storms that are seemingly relevant to their following flux enhancements can be merely coincidental. Additionally, there are numerous examples of electron enhancements that are not preceded/accompanied by substantial storm disturbances. Those events are usually associated with high-speed streams whose prolonged north-south fluctuating IMF drives sustained substorm activity without driving a large storm. During 1996 to 2006, we identified a total of 17 relativistic electron events that occurred with small *Dst* perturbations (> -50 nT), where relativistic electron event is defined as an event of flux increase by more than 2 orders of magnitude with a peak $> 2 \times 10^3$ cm^{-2} s^{-1} sr^{-1}, similar to *Kim et al*. [2006]. Considering that this flux increase criteria is much more rigorous than that for the high-flux storms, we see that large flux enhancements without accompanying magnetic storms occur quite frequently (i.e., 17 relativistic electron events with $Dst_{min} > -50$ nT versus 65 high-flux storms with $Dst_{min} < -50$ nT). As illustrated in Table 1, these nonstorm time electron events exhibit average features of solar wind and substorm activity during the first day of flux enhancements that are very similar to what was found for the high-flux storms in section 2. All these indicate that electron enhancements occur whenever solar wind/IMF conditions become favorable, and this is not dependent on the presence of a magnetic storm. Whether an electron event accompanies a storm or not is merely coincident.

Table 1. Average Conditions Associated With Geosynchronous Electron Enhancements[a]

	# of Events	Dst_{min} (nT)	Average V_{sw} (km/s)	Average N_{sw} (cm^{-3})	Average *AE* (nT)	Time of South B_z (Day)
Relativistic Electron Enhancements (REE), $Dst > -50$ nT	17	−24 to −48 (−43)	472–743 (611)	1.9–5.3 (3.1)	260–488 (332)	0.4–0.9 (0.6)
High flux storms	65	−50 to −393 (−104)	431–869 (617)	0.5–5.9 (2.8)	203–962 (423)	0.4–1.0 (0.6)

[a]Median is in parenthesis.

4. Summary and Conclusion

We have presented evidence that relativistic electron flux enhancements at geosynchronous orbit are produced by distinct solar wind drivers, which may be different from those that directly produce the main phase of geomagnetic storms and can occur without storm drivers. What is crucial for electron enhancements are sustained south-oriented or north-south fluctuating IMF B_z that drives sufficiently large *AE* activity, as well as small N_{sw} that likely leads to low relativistic electrons loss rate to the ionosphere and/or to the magnetopause for an extended time period. Specifically, almost all the abrupt, large electron flux increases in our data set, regardless of the presence of magnetic storms, took place under the condition of average $AE > 235$ nT and average $N_{sw} \leq 5\,cm^{-3}$. This results show that while conditions leading to electron enhancements can be preceded by conditions that lead to a storm, the storm itself is not the feature that gives rise to an enhancement. Furthermore, due to the relatively immediate electron response, examinations of detailed time profiles are necessary even in statistical studies, not only for correct determination of the relationship between storms and electron enhancements but also for precise determination of the key solar wind and magnetosphere driver(s) of enhancements.

The role of substorms for relativistic electron enhancements has been discussed in many studies [e.g., *Kim et al.*, 2000, 2006; *Lyons et al.*, 2005]. Prolonged substorm activity can continuously inject high-energy plasma sheet particles. The repetitive injection of those particles can contribute to growth of waves such as Pc5 ULF and whistler mode chorus and at the same time provide seed electrons that can be accelerated to MeV energies via wave-particle interactions [e.g., *Elkington et al.*, 1999; *Meredith et al.*, 2001, 2002]. It is well known that large-amplitude Alfvén fluctuations are ubiquitous within high-speed solar wind streams. Continuous excursions of southward B_z drive continuous substorm occurrence, so-called High Intensity Long Duration Continuous Auroral Activity [*Tsurutani and Gonzalez*, 1987]. Moreover, the time-fluctuating solar wind can help the solar wind electric field to penetrate more effectively to the inner magnetosphere, enhancing substorm activity, compared to steady solar wind conditions [*Garrett et al.*, 1974; *Kim et al.*, 2009; *Lyons et al.*, 2009]. Therefore, combined with the fact that high-speed streams are usually low-density solar wind, high-speed solar wind streams with fluctuating but predominantly southward IMF can provide the optimal environment for MeV electron generation. This would be the reason for the close correlation between high-speed streams and large electron enhancements in the geosynchronous region. However, we note that electron enhancements can also occur during nonhigh-speed streams, as long as the streams accompany the favorable N_{sw} and IMF conditions. Furthermore, we note here that while electron enhancements at geosynchronous orbit likely occur independently from storms, electron intensities in other regions of the radiation belts may have different dependences on storms. For example, it has been observed that large electron enhancements in the inner edge of the outer belt are closely related with the strength of a magnetic storm [e.g., *Zhao and Li*, 2013].

Acknowledgments

Work at UCLA was supported by NASA grant NNX14AD18G. The work at KASI in Korea was supported by "Planetary system research for space exploration" project and basic research funding from KASI. We thank J.H. King and N. Papatashvilli at AdnetSystems, NASA GSFC, and CDAWeb for providing the OMNI data and thank T. Onsager at NOAA SEC and CDAWeb for providing the electron flux data observed by GOES spacecraft. The GOES electron data and the OMNI data set of time-shifted solar wind and geomagnetic indices are available at http://cdaweb.gsfc.nasa.gov/istp_public/.

The Editor thanks Dae-Young Lee and an anonymous reviewer for their assistance in evaluating this paper.

References

Borovsky, J. E., and M. H. Denton (2009), Relativistic electron dropouts and recovery: A superposed epoch study of the magnetosphere and the solar wind, *J. Geophys. Res.*, *114*, A02201, doi:10.1029/2008JA0130128.

Bühler, P., and L. Desorgher (2002), Relativistic electron enhancements, magnetic storms, and substorm activity, *J. Atmos. Sol. Terr. Phys.*, *64*, 593–599.

Degtyarev, V. I., I. P. Kharchenko, A. S. Potapov, B. Tsegmed, and S. E. Chudnenko (2009), Qualitative estimation of magnetic storm efficiency in producing relativistic electron flux in the Earth's outer radiation belt using geomagnetic pulsations data, *Adv. Space Res.*, *43*, 829–836.

Elkington, S. R., M. K. Hudson, and A. A. Chan (1999), Acceleration of relativistic electrons via drift-resonant interaction with toroidal-mode Pc-5 ULF oscillations, *Geophys. Res. Lett.*, *26*(21), 3273–3276, doi:10.1029/1999GL003659.

Garrett, H. B., A. J. Dessler, and T. W. Hill (1974), Influence of solar wind variability on geomagnetic activity, *J. Geophys. Res.*, *79*, 4603–4610, doi:10.1029/JA079i031p04603.

Kim, H.-J., A. A. Chan, R. A. Wolf, and J. Birn (2000), Can substorms produce relativistic outer belt electrons?, *J. Geophys. Res.*, *105*(A4), 7721–7735.
Kim, H.-J., K. C. Kim, D.-Y. Lee, and G. Rostoker (2006), Origin of geosynchronous relativistic electron events, *J. Geophys. Res.*, *111*, A03208, doi:10.1029/2005JA011469.
Kim, H.-J., L. Lyons, S. Zou, A. Boudouridis, D. Y. Lee, C. J. Heinselman, and M. McCready (2009), Evidence that solar wind fluctuations substantially affect the strength of dayside ionospheric convection, *J. Geophys. Res.*, A11305, doi:10.1029/2009JA014280.
Kim, K. C., D.-Y. Lee, H.-J. Kim, L. R. Lyons, E. S. Lee, M. K. Ozturk, and C. R. Choi (2008), Numerical calculations of relativistic electron drift loss effect, *J. Geophys. Res.*, *113*, A09212, doi:10.1029/2007JA013011.
Kozyreva, O., V. Pilipenko, M. J. Engebretson, K. Yumoto, J. Watermann, and N. Romanova (2007), In search of a new ULF wave index: Comparisons of PC5 power with dynamics of geostationary relativistic electrons, *Planet. Space Sci.*, *55*, 755–769.
Lyons, L. R., D.-Y. Lee, R. M. Thorne, R. B. Horne, and A. J. Smith (2005), Solar wind-magnetosphere coupling leading to relativistic electron energization during high-speed streams, *J. Geophys. Res.*, *110*, A11202, doi:10.1029/2005JA011254.
Lyons, L. R., et al. (2009), Evidence that solar wind fluctuations substantially affect global convection and substorm occurrence, *J. Geophys. Res.*, A11306, doi:10.1029/2009JA014281.
Meredith, N. P., R. Horne, and R. Anderson (2001), Substorm dependence of chorus amplitudes: Implications for the acceleration of electrons to relativistic energies, *J. Geophys. Res.*, *106*, 13,165–13,178, doi:10.1029/2000JA900156.
Meredith, N. P., R. B. Horne, D. Summers, R. M. Thorne, R. H. A. Iles, D. Heynderickx, and R. R. Anderson (2002), Evidence for acceleration of outer zone electrons to relativistic energies by whistler mode chorus, *Ann. Geophys.*, *20*, 967–979.
O'Brien, T. P., R. L. McPherron, D. Sornette, G. D. Reeves, R. Friedel, and H. J. Singer (2001), Which magnetic storms produce relativistic electrons at geosynchronous orbit?, *J. Geophys. Res.*, *106*, 15,533–15,544, doi:10.1029/2001JA000052.
O'Brien, T. P., K. R. Lorentzen, I. R. Mann, N. P. Meredith, J. B. Blake, J. F. Fennell, M. D. Looper, D. K. Milling, and R. R. Anderson (2003), Energization of relativistic electrons in the presence of ULF power and MeV microbursts: Evidence for dual ULF and VLF acceleration, *J. Geophys. Res.*, *108*(A8), 1329, doi:10.1029/2002JA009784.
Reeves, G. D. (1998), Relativistic electrons and magnetic storms: 1992–1995, *Geophys. Res. Lett.*, *25*(11), 1817–1820, doi:10.1029/98GL01398.
Reeves, G. D., K. L. McAdams, R. H. W. Friedel, and T. P. O'Brien (2003), Acceleration and loss of relativistic electrons during geomagnetic storms, *Geophys. Res. Lett.*, *30*(10), 1529, doi:10.1029/2002GL016513.
Rostoker, G., S. Skone, and D. N. Baker (1998), On the origin of relativistic electrons in the magnetosphere associated with some geomagnetic storms, *Geophys. Res. Lett.*, *25*, 3701–3704, doi:10.1029/98GL02801.
Shprits, Y. Y., R. M. Thorne, R. Friedel, G. D. Reeves, J. Fennell, D. N. Baker, and S. G. Kanekal (2006), Outward radial diffusion driven by losses at magnetopause, *J. Geophys. Res.*, *111*, A11214, doi:10.1029/2006JA011657.
Tsurutani, B. T., and W. D. Gonzalez (1987), The cause of high-intensity long-duration continuous *AE* activity (HILDCAAs): Interplanetary Alfvén wave trains, *Planet. Space Sci.*, *35*, 405–412.
Zhao, H., and X. Li (2013), Inward shift of outer radiation belt electrons as a function of *Dst* index and the influence of the solar wind on electron injections into the slot region, *J. Geophys. Res. Space Physics*, *118*, 756–764, doi:10.1029/2012JA018179.